Plastic viscosity of cement mortar with manufactured sand as influenced by geometric features and particle size

Ren, Qiang; Tao, Yaxin; Jiao, Dengwu; Jiang, Zhengwu; Ye, Guang; De Schutter, Geert

DOI
10.1016/j.cemconcomp.2021.104163

Publication date
2021

Document Version
Final published version

Published in
Cement and Concrete Composites

Citation (APA)
Ren, Q., Tao, Y., Jiao, D., Jiang, Z., Ye, G., & De Schutter, G. (2021). Plastic viscosity of cement mortar with manufactured sand as influenced by geometric features and particle size. *Cement and Concrete Composites*, *122*, Article 104163. https://doi.org/10.1016/j.cemconcomp.2021.104163

Cement and Concrete Composites 122 (2021) 104163

Contents lists available at ScienceDirect

Cement and Concrete Composites

journal homepage: www.elsevier.com/locate/cemconcomp

Plastic viscosity of cement mortar with manufactured sand as influenced by geometric features and particle size

Qiang Ren [a,b], Yaxin Tao [b], Dengwu Jiao [b], Zhengwu Jiang [a,*], Guang Ye [b,c], Geert De Schutter [b,**]

[a] Key Laboratory of Advanced Civil Engineering Materials of Ministry of Education, School of Materials Science and Engineering, Tongji University, 4800 Cao'an Road, Shanghai, 201804, China
[b] Magnel-Vandepitte Laboratory, Department of Structural Engineering and Building Materials, Ghent University, Technologiepark-Zwijnaarde 60, Ghent, 9052, Belgium
[c] Microlab, Faculty of Civil Engineering and Geosciences, Delft University of Technology, Stevinweg 1, 2628CN, Delft, the Netherlands

ARTICLE INFO

Keywords:
Plastic viscosity
Geometric features
Manufactured sand
Packing fraction
Relative paste film thickness

ABSTRACT

This paper investigates the plastic viscosity of cement mortar with manufactured sand (MS) concerning the influences of geometric features and particle size of MS. The geometric features, including overall shape, angularity and roughness, of MS with various particle sizes were evaluated by aspect ratio, convexity area ratio, convexity perimeter ratio and circularity. The plastic viscosity of cement mortar was calculated based on the Bingham model. Results show that the combined effects of overall shape, angularity and roughness provide coarser MS particles with lower circularity. In terms of relative plastic viscosity, Robinson model shows optimal fittings for all mixtures and is thus used to determine the packing fraction of MS under shearing. From the particle packing viewpoint, shear-induced orientation increases the packing fraction of non-spherical MS particles from the random loose packing fraction and the influence is increasingly prominent with the decrease of circularity. The relative volume fraction is an important parameter influencing the relative plastic viscosity of mixtures with MS while the relative paste film thickness (R_PFT), calculated from the real packing fraction and specific surface area (SSA), is found as the dominating factor. The dependence of plastic viscosity of cement mortar on geometric features and particle size of MS can be attributed to their influences on the packing fraction and SSA of particles.

1. Introduction

There has been increasing interest in using manufactured sand (MS) as fine aggregate for mortar or concrete to overcome the increasing deficiency in river sand and thus alleviate the environmental problems caused by overexploitation of river sand. Unlike river sand, MS is the product of rock crushing, which creates grains with distinctive geometric features, depending on the parent rock composition, fracture mode, coordination number during crushing, and the reduction ratio [1–4]. The formation history of manufactured sand tends to produce angular, sharped edged and rough particles. The shape and texture of manufactured sand could improve the strength of concrete due to better interlocking connections of sand-paste or particle-particle [5–7]. However, manufactured sand was found to cause poorer workability in mortar or concrete [8–10].

Westerholm et al. measured the rheology of mortar mixtures with various MS and found that the plastic viscosity of mortar increased almost three times as MS became increasingly elongated, which was attributed to the increased particle interference between non-spherical particles [11]. Thus, the influence of MS on plastic viscosity of cement mortar was demonstrated as a particle shape effect [11,12]. This proposal was supported by similar results showing that any deviation from a spherical particle shape results in an increased viscosity if the measurement is done at the same phase volume [4,13].

From the viewpoint of particle packing, the workability or rheology of mortar was demonstrated as dominated by the packing fraction of sand [14]. Thus the impact of particle shape on rheology may be captured through its effect on the packing fraction of particles while MS normally has lower packing fraction than river sand due to poorer particle shape [15–17]. By increasing the paste volume, negative effects due to decreased packing fraction of poorly shaped aggregates can be eliminated or significantly reduced [11]. It follows that a larger volume

* Corresponding author.
** Corresponding author.
E-mail addresses: jzhw@tongji.edu.cn (Z. Jiang), Geert.DeSchutter@Ugent.be (G. De Schutter).

https://doi.org/10.1016/j.cemconcomp.2021.104163
Received 11 June 2020; Received in revised form 28 June 2021; Accepted 29 June 2021
Available online 1 July 2021

of paste is required to attain adequate rheology for mortar mixture with MS [5,18]. Therefore, the influence of particle shape on rheology may be attributed to its influence on the packing properties of particles as well [17,19].

Meanwhile, it is well acknowledged that it is the excess paste that contributes to the workability of cement-based materials given that it forms lubricating layer surrounding each particle [20–22]. Similar results were found that water film thickness [23–25], paste film thickness [26,27] and mortar film thickness [28,29] influence the rheology and workability of paste, mortar and concrete respectively. More precisely, the yield stress of mortars decreases exponentially with the increase of paste film thickness [28]. Particle shape of sand influences its surface area in addition to its influence on the packing fraction, thus influencing the paste film thickness. As a result, the influence of particle shape on the rheology of mortar may be due to the paste film thickness variation as influenced by particle shape.

It thus can be summarized that particle shape may influence the rheology of mortar in various ways, including the particle shape itself and its influences on the packing fraction and paste film thickness. It needs to be noted that MS has a wide particle size distribution and the geometric features of particle with various sizes are not identical [3,17]. As a result, roles of particles with various dimensions in the rheology of cement mortar mixtures may be different.

Therefore, this paper evaluates the roles of MS particles in the rheology of cement mortar concerning the geometric features and particle size. MS particles with various sizes are obtained by sieving. Spherical glass beads (GB) are employed for comparison. The geometric features of sands, including overall shape, angularity and roughness, are analyzed based on image processing techniques. Plastic viscosity is calculated based on the Bingham model and used as the rheology index of mixture given that the influence of particle shape of aggregates on the plastic viscosity is more prominent than the yield stress [30]. The plastic viscosity of mixtures is discussed from the viewpoints of packing fraction and paste film thickness. The essential roles of geometric features and particle size of MS are analyzed.

2. Experiment

2.1. Materials and mix proportions

Type I Portland cement (CEM I 52.5 N) was used in all mixtures. The physical properties and chemical compositions are summarized in Table 1 and Table 2 respectively. The particle size distribution was measured by the laser diffraction method (Mastersizer 2000) and is shown in Fig. 1.

MS with the maximum diameter of 2.00 mm was purchased from an industrial company in Ghent, Belgium. It was produced from the Doornik limestone rock by a vertical shaft impact crusher. Five fractions (0.25/0.5 mm, 0.50/1.00 mm, 1.00/1.25 mm, 1.25/1.40 mm and 1.40/2.00 mm) of particles were obtained by dry sieving. Glass bead, with the diameter from 0.30 mm to 0.80 mm, was purchased from an industrial company in the Netherlands.

In the mortar mixtures, the water to cement ratio was kept at 0.50. No superplasticizer was used in case MS may have adsorption capability of superplasticizer, to emphasize the influence of geometric features of MS. The volume fraction of sand in mortar mixtures was varied between zero and the maximum value that could be considered in view of proper rheometer testing. Cement and water were mixed in a planetary mixer at a rotational speed of 140 rpm for 60 s, during which sand was added within 30 s in case of mortar mixtures. Afterwards, mixtures were mixed at a rotational speed of 280 rpm for 30 s, followed by a stop of mixing process during 30 s to manually homogenize the mixtures. Mixtures for rheology testing underwent a final mixing cycle at a rotational speed of 280 rpm for 120 s.

2.2. Property measurements of sands

2.2.1. Packing fractions

When studying the rheological properties of mixtures as a function of volume fraction of particles, the packing properties are significant. Noted particle packing is not an intrinsic characteristic of aggregates since it depends on the compaction method and the applied energy. Thus both the random loose packing fraction and the random dense packing fraction are employed. The random loose packing fraction ($\phi_{m,exp}$) is calculated from the ratio of the random loose packing density ($\rho_{s,p}$) to the apparent density ($\rho_{s,a}$), shown below.

$$\phi_{m,loose} = \frac{\rho_{l,p}}{\rho_{s,a}} \tag{1}$$

The apparent density of sand was measured from a pycnometer while the measurement of random loose packing density was modified from BS EN 1097-3:1998 [31] by using a container as shown in Fig. 2. Firstly, sand particles were poured in the container slowly to alleviate the influence of energy on the random loose packing fraction [32]. Then the sand collected in the container was gently levelled. The random loose packing density was determined from mass of sand in the container divided by the volume of the container.

Different from the loose packing fraction, the dense packing fraction is dependent on the vibration conditions. Hafid et al. proposed that the vibration with a frequency of 50 Hz and amplitude of 0.5 mm provided the best dense packing fraction result. However, it was checked by authors that better dense packing fraction can be provided by the low frequency with high amplitude (LFHA), provided by the jolting apparatus as specified in ISO 679:2009(E) [33], which has a frequency of 1 Hz and amplitude of 15.0 mm. Then the dense packing fraction can be calculated as the ratio between the dense packing density ($\rho_{d,p}$) and the apparent packing density ($\rho_{s,a}$) of particles, shown below.

$$\phi_{m,dense} = \frac{\rho_{d,p}}{\rho_{s,a}} \tag{2}$$

2.2.2. Geometric features and specific surface area

Digital image processing (DIP) has gained popularity and is widely used for the characterization of geometric characteristics. Particle morphology is commonly inferred from 2D images obtained by optical microscopy [34,35] and laser beam systems [36], or 3D images obtained from laser diffraction [37] and X-ray computed tomography [38,39]. 3D image based methods are able to provide more detailed information on the particle shape, angularity and surface texture while 2D image based methods are more easy-to-perform whereas with possibility of bias on the evaluation of geometric features due to the loss of the features on the third dimension.

Based on the captured images, the aggregate geometric features like overall shape, angularity and texture can be quantified. In view of availability of apparatus, 2D images are used in this study. The random sections of particles were used to alleviate the subjectivity and bias in

Table 1
Physical properties of cement.

Water requirement (%)	Setting time		Stability (mm)	Blaine specific surface area (m^2/kg)	Apparent density (kg/m^3)	Sieve residue 200 μm (%)
	Initial	Final				
29	3h25min	4h14min	<1	408	3160	<0.5

Table 2
Chemical compositions of cement (%).

CaO	SiO_2	Al_2O_3	Fe_2O_3	MgO	Na_2O	K_2O	SO_3	Cl^-	LOI	Insoluble
64.3	18.3	5.2	4.0	1.4	0.32	0.43	3.5	0.06	2.3	0.4

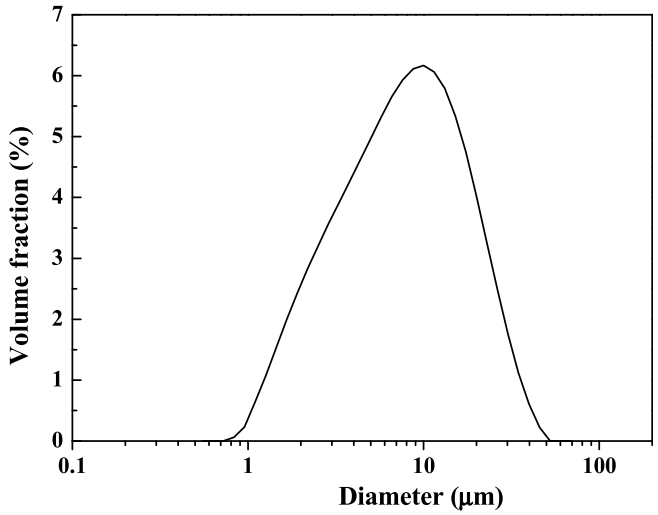

Fig. 1. Particle size distribution of cement.

assessment of 3D object involved by 2D measurement. Sand particles (Fig. 3a) were washed and dried before being impregnated into epoxy resin (EpoFix Resin, Struers Inc., USA) in a silicon mold. Fluorescent dye (EpoDye, Struers Inc., USA) was also used to increase the contrast between objects and background. The hardened sample (Fig. 3b) was then polished by silicon paper #180, #320, #1200 and 2000# successively until no visible notch can be observed at each localized area. A smooth surface with abundant exposed particles can be obtained after these procedures. Finally, the optimal microscope (Leica S8 APO, Fig. 3c) was used to capture the section image of particles. The image processing and geometric parameters calculation were performed by MATLAB.

The geometric properties of a particle can be fully expressed in terms of three independent properties at different length scales: overall shape (large scale) [40,41], angularity (intermediate scale) [34,42], and roughness (fine scale) [43–45]. Even though the length (L), width (W) and thickness (T) are widely used to express the particle shape of particles via parameters like L/W and L/T [3,35,46]. They are not able to describe the fine scale features of particles, like angularity and roughness.

In this paper, aspect ratio (ASR) of the fitted ellipse that has the same normalized second central moments as the region (shown in Fig. 4a), is used to evaluate the overall shape of particles based on the consideration that MS particles can be approximated as ellipsoid [47–49]. ASR is calculated as follows.

$$ASR = \frac{L_{maj}}{L_{min}} \tag{3}$$

where L_{maj} and L_{min} are the major and minor axes of the fitted ellipse respectively.

Convex hull is the smallest convex polygon that can contain the object region. The convexity area ratio (CAR), calculated as the area ratio between the object region and its convex hull (Fig. 4b), is employed

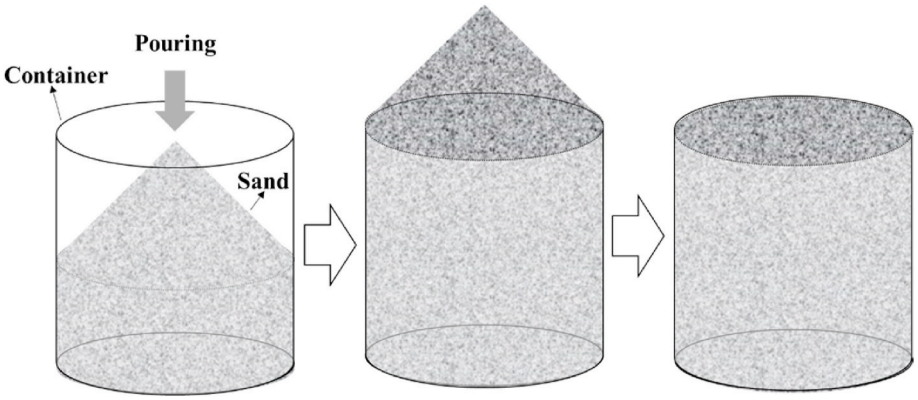

Fig. 2. Measurement of packing density of sand.

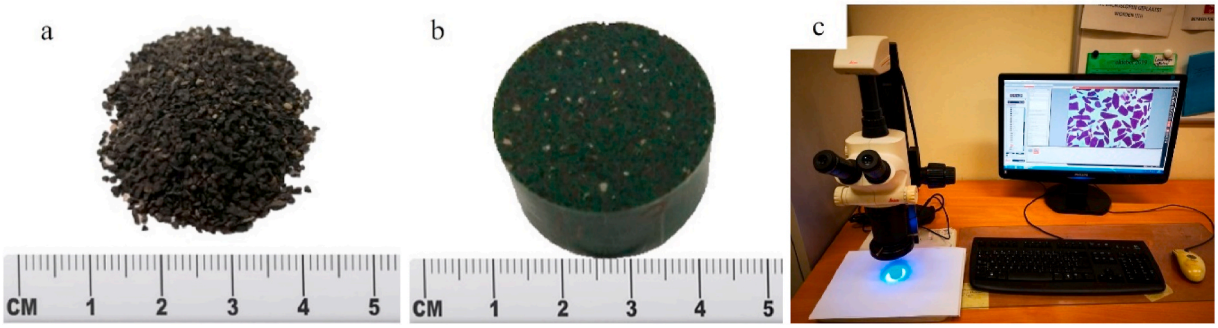

Fig. 3. Sand particles (a) and sample for image acquisition (b) under optical microscope (c).

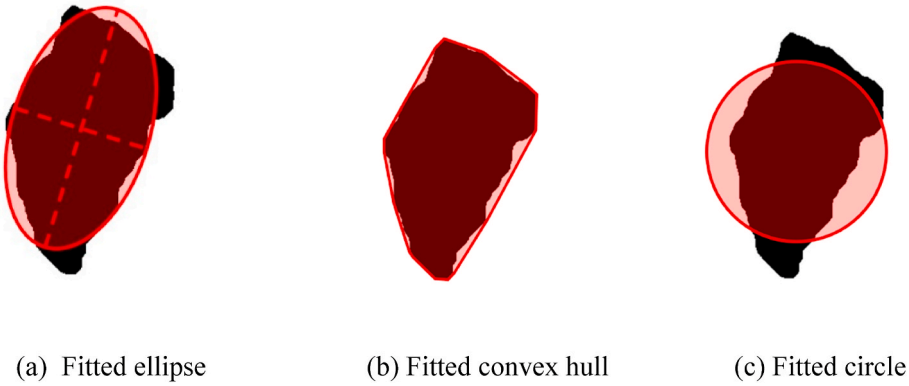

Fig. 4. Illustration of particle shape characterization.

to measure the angularity of sand [34], which can be shown as follows.

$$CAR = \frac{A}{A_{con}} \tag{4}$$

where A and A_{con} are the areas of the object region and its convex hull, respectively.

In terms of surface roughness, convexity perimeter ratio (CPR), defined as the perimeter ratio between the convex hull (Fig. 4b) and the object region [17,50], is used and calculated as follows.

$$CPR = \frac{P}{P_{con}} \tag{5}$$

where P and P_{con} are the perimeters of the object region and its convex hull, respectively.

Circularity (CIR) is to evaluate the similarity between the particle and the perfect sphere, which is influenced by the overall shape, angularity and surface roughness of particles. Circularity is determined as the area ratio between the object and the equivalent circle with the same perimeter (Fig. 4c), expressed as Eq. (6).

$$CIR = \frac{4\pi A}{P^2} \tag{6}$$

where A and P are the area and perimeter of the object region, respectively.

Specific surface area (SSA) is a comprehensive evaluation of particle size, shape, angularity and surface roughness of aggregate [51,52]. SSA of particles were measured by the random sectioning method in this study, which has proved by the authors with favorable accuracy compared to the computed tomography method. The SSA of particles can be calculated as Eq. (7). Detailed information concerning the measurement of SSA can be found in Ref. [53].

$$\mathrm{SSA} = \frac{4}{\pi}\frac{\bar{l}}{\bar{A}} \tag{7}$$

where $\bar{l}$ and $\bar{A}$ are the average perimeter and average area of random sections of particles respectively.

2.3. Rheology measurement of mixtures

A rheometer (MCR 102, Anton Paar, Austria) is used for rheological tests, as presented in Fig. 5a. The measuring system consists of a unit cell (Fig. 5b) with a rotational spindle geometry (Fig. 5c). The surface of the geometry is covered with sandpaper and the unit cell is ribbed to alleviate the risk of slippage. The ratio between the cylinder gap and the particle size of the coarsest sand is 7.25, which is high enough for a reliable result [54]. The protocol of rheology test is shown in Fig. 6. The shear rate stepwise increases from 0 1/s to 100 1/s by ten steps, followed by a stepwise decreasing shear rate from 100 1/s to 0 1/s. Each step of shearing is maintained for 10 s to achieve an equilibrium state. After the rheological test, the mortar in the cylinder was checked, and no obvious sedimentation or bleeding was observed. Three samples were prepared and tested for each mixture.

The results obtained in the descending stage are generally more consistent and repeatable, which is well described by the Bingham model in this study. Therefore, the linear portion of the descent curve is used to calculate the plastic viscosity, η_{pl} (Pa/s), of mixtures [55].

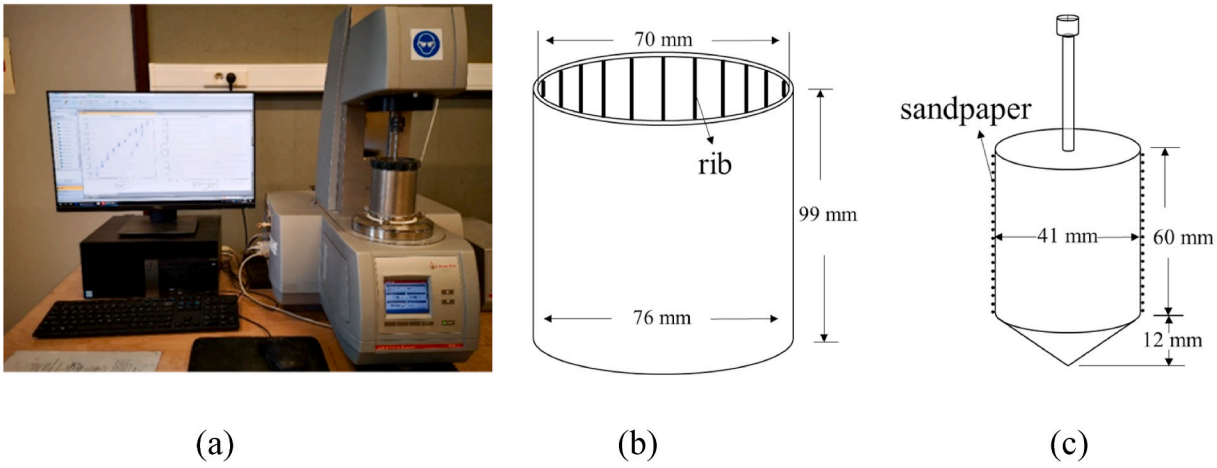

Fig. 5. Setup for rheology test: (a) Rheometer, (b) Unit cell, and (c) Spindle geometry.

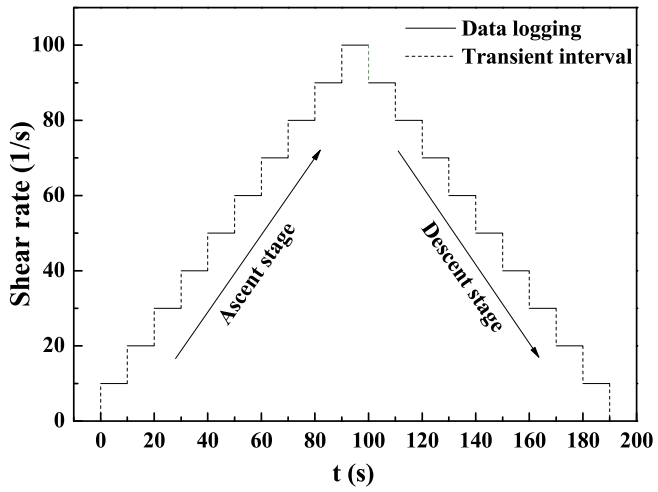

Fig. 6. The protocol of rheology test.

$$\tau = \tau_0 + \eta_{pl}\frac{d\gamma}{dt} \tag{8}$$

where τ (Pa) is the shear stress at the shear rate of $\frac{d\gamma}{dt}$ (1/s), τ_0 (Pa) is the yield stress.

The relative plastic viscosity, η_r, of mixture is used to evaluate the impacts of sands on the plastic viscosity of mixtures, calculated by Eq. (9).

$$\eta_r = \frac{\eta_{pl,m}}{\eta_{pl,p}} \tag{9}$$

where $\eta_{pl,m}$ and $\eta_{pl,p}$ are the plastic viscosity of cement mortar and its corresponding cement paste respectively.

3. Geometric features of MS and GB

The geometric features, including aspect ratio (Eq. (3)), convexity area ratio (Eq. (4)), convexity perimeter ratio (Eq. (5)) and circularity (Eq. (6)), of MS and GB are shown in Fig. 7. For spherical GB, all these four parameters have the value of 1.0. MS particles have aspect ratios twice higher than GB (Fig. 7a), indicating that MS particles have a highly anisotropic overall shape. Besides, coarser MS particles show higher anisotropy, demonstrated by the increased aspect ratio with the increase of particle size. It can be seen from Fig. 7b that MS particles have convexity area ratios lower than 1.0, which indicates the angular feature of

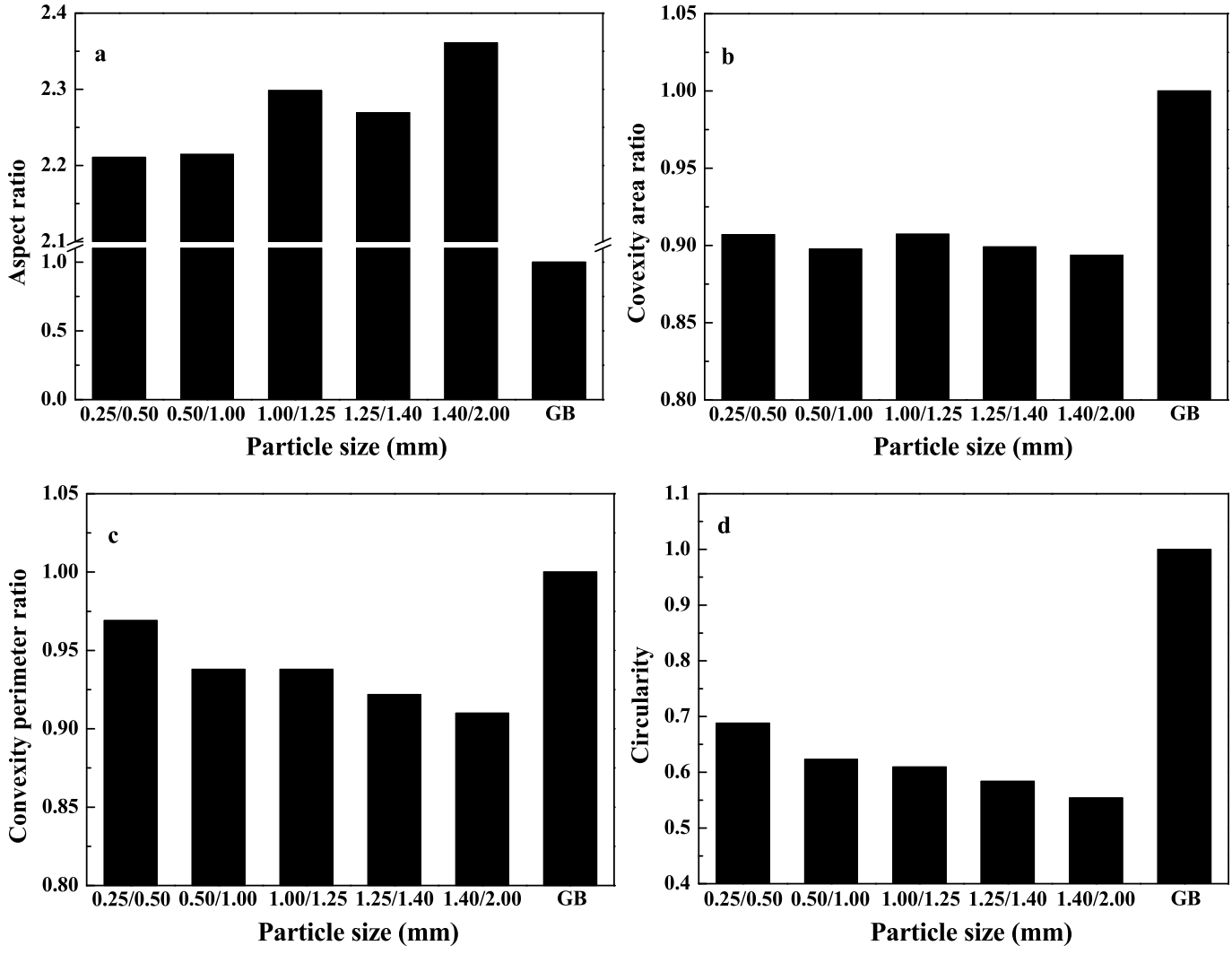

Fig. 7. Geometric features (a) Aspect ratio, (b) Convexity area ratio, (c) Convexity perimeter ratio, and (d) Circularity.

MS particles. In addition, it can be inferred from the quite similar convexity area ratios among various particle sizes that MS particles have similar angularity, independent of the particle size. However, the convexity perimeter ratio is found to decrease with increasing MS particle size (Fig. 7c). Thus it is inferred that coarser MS particles have rougher surface.

Aspect ratio, convexity area ratio, and convexity perimeter ratio are independent parameters to evaluate the geometric features of particles from different scales while circularity is a comprehensive evaluation, which is influenced by the former three parameters. Normally, the particle with higher anisotropy (higher aspect ratio), higher angularity (lower convexity area ratio), and higher roughness (lower convexity perimeter ratio) shows more non-spherical features. The additive effect of increased aspect ratio and decreased convexity perimeter ratio, with negligible influence from the comparable convexity area ratio, makes coarser MS particles present more remarkable non-spherical features, which is manifested by the decreased circularity in Fig. 7d.

4. Relative plastic viscosity of mortar with manufactured sand

4.1. Relative plastic viscosity versus volume fraction

The relative viscosity of mortar with various volume fractions of sand is shown in Fig. 8. Obviously, all mixtures have an increasing relative plastic viscosity as the volume fraction of sand increases. In addition, mixtures with MS exhibit higher relative plastic viscosity than mixtures with spherical GB at each volume fraction. Interestingly, mixtures containing MS particles with higher anisotropy (higher aspect ratio, lower convexity perimeter ratio, lower circularity) show lower relative plastic viscosity. This result is in contradiction with the trend mostly reported in literature [4,11,17]. Particles with high specific surface area require more free paste to lubricate the surface of the particles, i.e. size effect, showing a negative impact on the plastic viscosity. On the other hand, particles with more isotropy have a positive influence on the rheological properties (shape effect). The unexpected observation in this study could be caused by the predominant size effect of fine particles over their shape effect.

It is widely considered that the relative plastic viscosity of mortar is governed by the volume fraction of sand, which was first described by the viscosity equation of Einstein [56].

$$\eta_r = 1 + [\eta]\phi \tag{10}$$

where η_r is the relative plastic viscosity, ϕ is the volume fraction of the sand particles in the mixtures, $[\eta]$ is the intrinsic viscosity of particles. At low particle volume fractions, the particle-fluid or particle-particle interactions are mainly hydrodynamic. By contrast, at relatively high concentrations, direct contacts between solid particles may occur and the frictional contacts start to dominate the rheological behavior, resulting in a significant deviation of viscosity from Einstein equation [57]. Based on the Einstein viscosity equation, various models have been proposed to describe the volume fraction dependence of the relative viscosity of concentrated suspensions, which can be summarized in Table 3.

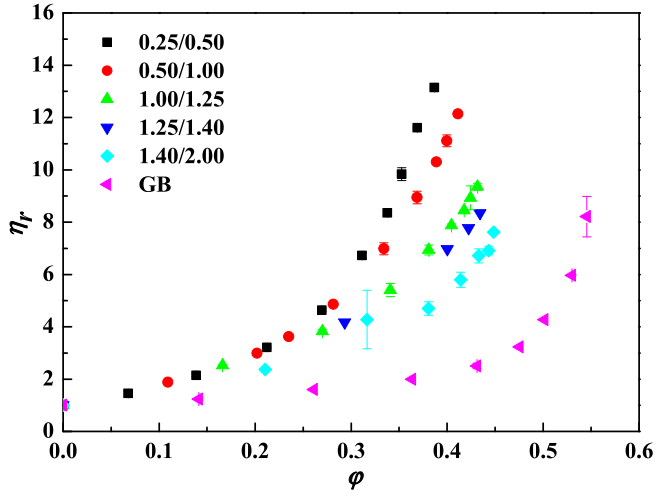

Fig. 8. Relative plastic viscosity as a function of volume fraction (ϕ) of sand in mortar.

All models in Table 3 are used to fit the points of relative plastic viscosity against volume fraction in Fig. 8. The fitting results are shown in Fig. 9 and Table 4. It needs to be mentioned that the lower and upper boundaries of maximum packing fractions fitted based on experimental result ($\phi_{m,fit}$) are 0 and 0.80 respectively. In case there might be mathematical solutions outside this range, those cannot exist in real case. The boundaries are determined based on the consideration that the maximum packing fraction of sand in mortar can barely reach 0.80. This means fitting cannot occur in real case if either of the boundaries is reached. It can be observed from Fig. 9 that most models show quite similar trends compared with the experimental results for all mixtures, indicating that all models seem applicable to all mortar mixtures with MS and GB. Specifically, it can be seen from Table 4 that the relative plastic viscosity of mortar with GB fits well with Krieger-Dougherty model, which is the most widely used model. However, this model is not applicable to several mixtures with MS when the boundary of 0.80 is reached. Besides, Maron-Piece model shows good fitting results for mixtures with MS whereas it cannot be used for mixture with GB. For Mooney model and Eilers model, boundary of 0.80 is reached as well for several or even all mixtures with MS, making them not suitable for mixtures with MS. Therefore, above four models cannot fit mixtures with MS or GB simultaneously. However, from Fig. 7e and fitted parameters in Table 4, rather favorable fittings are provided by Robinson model. Therefore, Robinson model can be used to excellently fit the relative plastic viscosity of all mortar mixtures with MS or GB.

It is generally accepted that the non-Newtonian behavior of dense suspensions results from changes in the microstructure of suspensions under shearing [64]. For suspensions with spherical particles, the microstructure is determined by the particle size distribution and positions of the suspended particles relative to each other. The particle shape is an additional factor to define the microstructure of suspensions in the case of non-spherical particles. Therefore, mortar mixtures with non-spherical MS show different relative plastic viscosity results from mixtures with spherical GB. From rheological viewpoint, it is widely recognized that there are four kinds of forces coexistent to various degrees in flowing mortar mixtures [65]: hydrodynamic, Brownian, colloidal and particle collision forces. Hydrodynamic force exists in all flowing suspensions and arises from the relative motion of particles to the surrounding fluid. The Brownian force is the ever-present thermal randomizing force, that can however be neglected for conventional cementitious materials without chemical admixtures or ultrafine additives. Colloidal force is the potential force and is elastic in nature. MS

Table 3
Relative plastic viscosity models of concentrated suspensions.

Model	Equation	Reference
Krieger-Dougherty model	$\eta_r = \left(1 - \frac{\phi}{\phi_M}\right)^{-[\eta]\phi_M}$ (11)	[58]
Mooney model	$\eta_r = \exp\left(\frac{[\eta]\phi}{1 - \phi/\phi_M}\right)$ (12)	[59]
Maron-Piece model	$\eta_r = \left(1 - \phi/\phi_M\right)^{-2}$ (13)	[60,61]
Robinson model	$\eta_r = 1 + [\eta]\left(\frac{\phi}{1 - \phi/\phi_M}\right)$ (14)	[62]
Eilers model	$\eta_r = \left[1 + \frac{1}{2}[\eta]\left(\frac{\phi}{1 - \phi/\phi_M}\right)\right]^2$ (15)	[63]

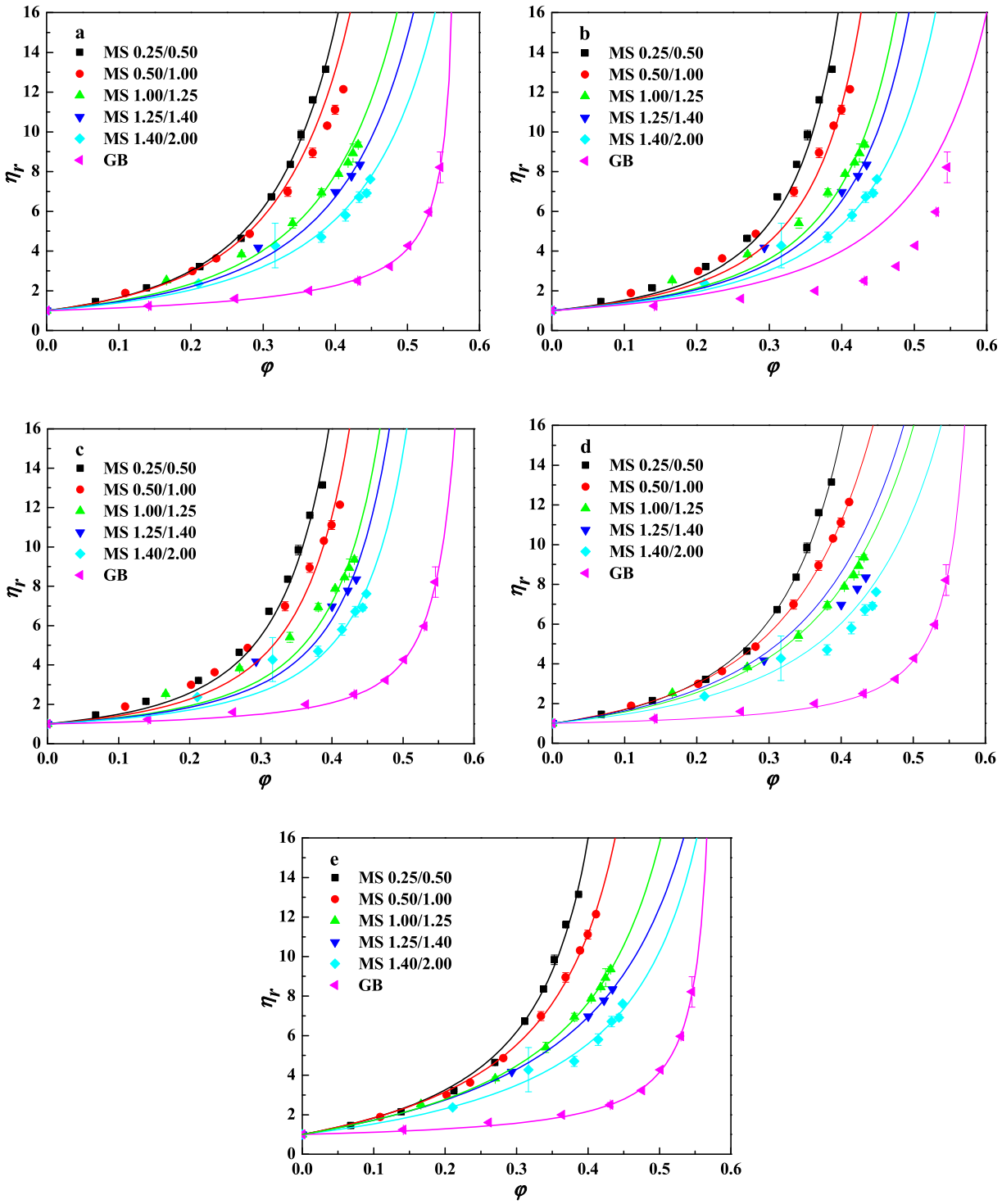

Fig. 9. Fitting of relative plastic viscosity of mixtures based on (a) Krieger-Dougherty model, (b) Maron-Piece model, (c) Mooney model, (d) Eilers model, and (e) Robinson model. Error bars are shown unless they are smaller than the symbol.

particles have no influence on the composition of cement paste matrix, thus the colloidal force is not altered by sand. Only the hydrodynamic force is affected due to sand [66]. It needs to be mentioned that at concentrated regime, sand particle crowding produces collisions and the probability of collision increases with increasing volume fraction. Therefore, the type of particle-particle or particle-matrix interactions vary with respect to the particle volume fraction present in the system. At low volume fractions, these interactions can be hydrodynamic. At higher volume fractions, direct contact can occur among sand particles, which leads to the transition of particle interactions from hydrodynamic to frictional regime and induces considerable amount of solid contacts throughout the suspension [57]. From Fig. 9e, η_r of the mixture with GB shows negligible increase until ϕ up to 0.50, followed by a dramatic increase. The negligible increase is attributed to weak influence of hydrodynamic force of spherical particles on the plastic viscosity of mixtures while the dramatic increase represents the dominating effect of particle collisions. However, mixtures with MS present higher η_r and higher increasing rates (the slopes of tangent lines) even at relatively

Table 4
Fitted parameters based on various models.

Model	Parameter	0.25/0.50	0.50/1.00	1.00/1.25	1.25/1.40	1.40/2.00	GB
Krieger-Dougherty model	$\phi_{M\phi_{m,fit}}$	0.73	0.80	0.80	0.80	0.80	0.57
	$[\eta]$	4.70	4.64	3.71	3.43	3.10	1.19
	R^2	0.998	0.900	0.985	0.980	0.965	0.999
Maron-Piece model	$\phi_{m,fit}$	0.53	0.57	0.63	0.66	0.70	0.80
	R^2	0.982	0.968	0.967	0.970	0.968	0.266
Mooney model	$\phi_{m,fit}$	0.80	0.80	0.80	0.80	0.80	0.68
	$[\eta]$	3.54	3.06	2.46	2.30	2.02	0.75
	R^2	0.984	0.952	0.924	0.917	0.914	0.996
Eilers model	$\phi_{m,fit}$	0.61	0.73	0.8	0.8	0.8	0.62
	$[\eta]$	5.00	5.34	4.48	4.82	3.64	0.79
	R^2	0.998	0.999	0.993	0.511	0.907	0.997
Robinson model	$\phi_{m,fit}$	0.48	0.55	0.63	0.68	0.66	0.59
	$[\eta]$	6.62	6.83	6.07	6.16	4.55	0.93
	R^2	0.995	0.998	0.999	0.999	0.982	0.998

low concentration. This is partially due to the hydrodynamic influence of non-spherical particles, which makes the local flow around a non-spherical particle more tortuous than that around a spherical particle [67]. Besides, the orbit of a rotating non-spherical particle encloses a greater volume for potential interactions than that of a spherical particle, making non-spherical particles a higher probability of collision than spherical ones [68]. Collision between MS particles happens even at low volume fractions. Therefore, mixtures with MS exhibit higher increasing rate of η_r even at low volume fractions. This is also the reason why the transition of particle interactions from hydrodynamic to frictional regime is not obvious for mixtures with MS.

Relative volume fraction is used to estimate the influence of packing fraction, which is calculated as the ratio of volume fraction of sand in mixtures to the packing fraction from the Robinson model fitting. Fig. 10 shows the variations of relative plastic viscosity under various relative volume fractions. It can be observed η_r results among mixtures with various MS sands in Fig. 10 present relatively good convergence even though η_r of the mixture with GB shows different trend compared to those with MS. The disagreement between mixtures with MS and GB is considered as the hydrodynamic influence of geometric features. The non-spherical features of MS increase the plastic viscosity even at low relative volume fraction. In addition, the convergence of η_r among mixtures with MS demonstrates that the influences of geometric features and particle size of MS on the relative plastic viscosity may be mainly attributed to their influences on the packing fraction of MS particles. However, since most of the deviations of η_r are relatively small, there is still a certain divergence among mixtures with MS. The small divergence may be attributed to the combined effects of hydrodynamic influence of geometric features, and the surface area as influenced by geometric features and particle size.

In terms of the packing fraction, it is to be noted that $\phi_{m,fit}$ is the real packing fraction that sand particles in the mixture can approach under the applied shearing condition. When the volume fraction of sand in mixture reaches $\phi_{m,fit}$, paste just fills the packing voids between particles and there is no excess paste for lubricating, under which condition the plastic viscosity of mixture is infinite and so is the relative plastic viscosity. The fitted packing fractions of sand are drawn as a function of the experimental loose packing fraction ($\phi_{m,loose}$) and dense packing fraction ($\phi_{m,dense}$), illustrated in Fig. 11. It is obvious that the fitted packing fraction of the spherical GB is quite close to the loose packing fraction, but slightly lower than the dense packing fraction. For non-spherical MS, all packing fractions from fitting are rather higher than the corresponding loose packing fractions whereas partial MS particles have fitted packing fractions higher than the dense packing fractions. Therefore, the random loose packing fraction can be taken as the real packing fraction of spherical particles under shearing while the real packing fraction of non-spherical particles under shearing is higher than its random loose packing fraction. The non-spherical particles tend to be oriented with respect to the streamlines during shearing, which may provide non-spherical particles with higher packing fraction than the

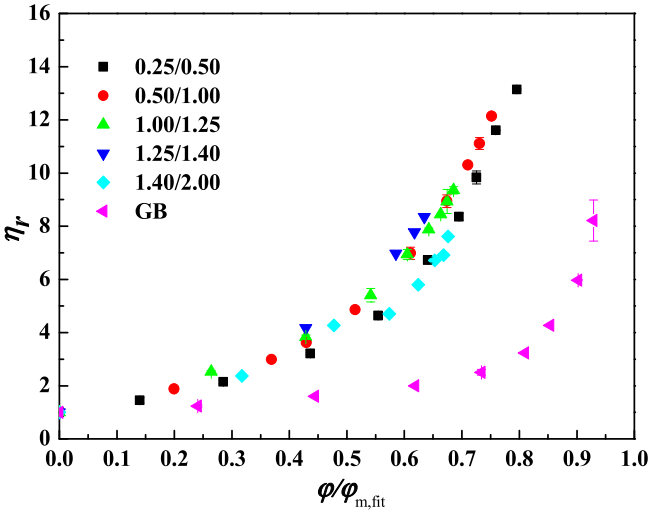

Fig. 10. Relative plastic viscosity as a function of relative volume fraction of sand based on fitted packing fraction from Robinson model.

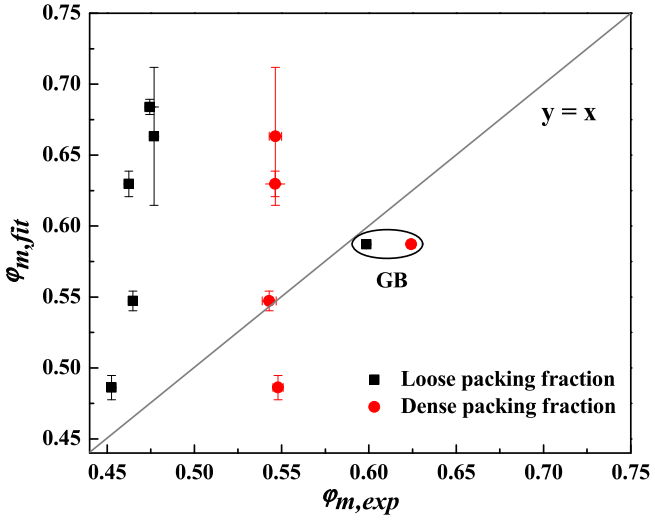

Fig. 11. Fitted packing fractions as a function of random loose packing fractions of sand.

loose packing fraction [69–71].

The rate of increment (α) is employed to evaluate the increment of packing fraction due to shearing, calculated as follows.

$$a = \frac{\phi_{m,fit} - \phi_{m,loose}}{\phi_{m,loose}} \tag{16}$$

Fig. 12 exhibits the rate of increment of packing fractions versus the circularity of particles. It is seen that the rate of increment of packing fraction is around zero at the circularity of 1.0 and increases with the decrease of circularity. This demonstrates that sand with more non-spherical shape has higher increment of packing fraction due to the orientation under shearing.

4.2. Relative plastic viscosity versus paste film thickness

The theory behind the Robinson model is that the relative plastic viscosity is not only proportional to the volume fraction of the particles, but also inversely proportional to the volume of free liquid in the suspension [62]. Similarly, Powers proposed the excess paste theory by postulating that it is the excess paste that contributes to the workability of mortar and concrete [72]. The free liquid introduced by Robinson and the excess paste proposed by Powers, despite of different names, share the same notion that the excess fluid, no matter in liquid form or in paste form, is one of the major factors affecting the rheological behavior of fluids with suspended particles such as mortar and concrete. Apart from the packing density and excess fluid, it was found that solid surface area of particles also exhibits great effect on the flowability and rheological properties of cement paste/mortar/concrete [26,73]. As a result, in addition to the packing fraction, paste film thickness was also considered as the dominating factor of the rheology of mortar since only the excess paste contributes to the rheology [74–77]. The thickness of excess paste was considered constant regardless of the dimension of aggregates [78]. Thus the average paste film thickness (PFT) of mortar mixtures can be calculated from the volume fraction and the real packing fraction of sand, expressed as Eq. (17).

$$\mathrm{PFT} = \frac{(1-\phi) - (1-\phi)\cdot\phi_{m,fit}}{\phi \cdot SSA} \tag{17}$$

where *SSA* is the volumetric specific surface area of sand.

The η_r results as a function of PFT are shown in Fig. 13. As expected, η_r of all mixtures increases as PFT decreases. To be specific, η_r increases gently first as PFT decreases, followed by a drastic increase when PFT decreases below a certain value. Besides, it can be observed that not all

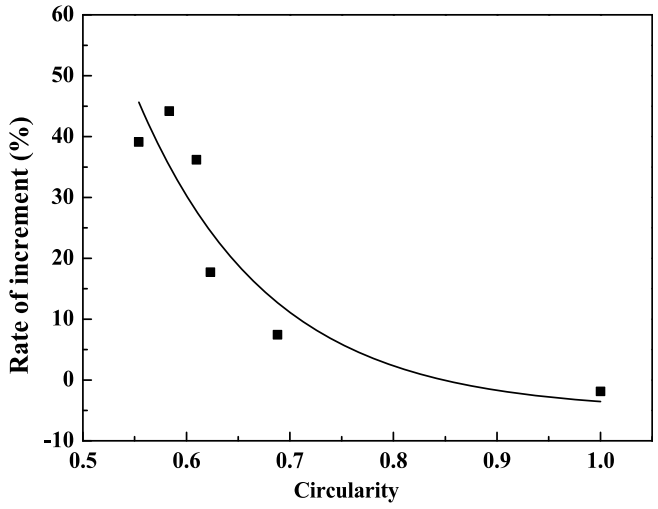

Fig. 12. Rate of increment of packing fraction as a function of the circularity of particles.

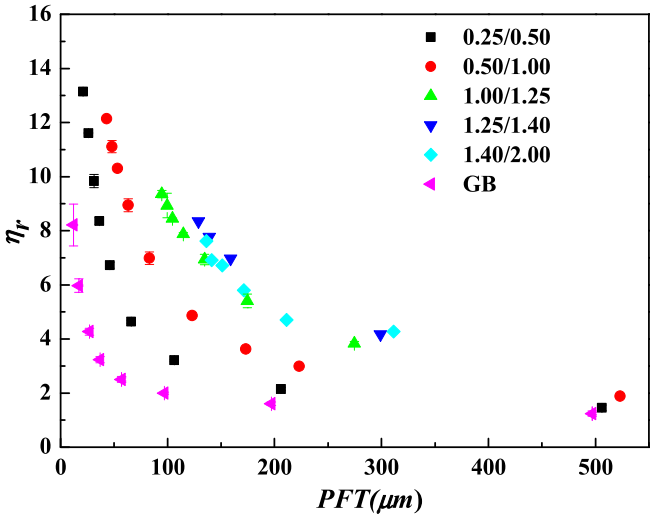

Fig. 13. Relative plastic viscosity of mixtures with various PFT.

mixtures show the identical quantitative relationship between η_r and PFT according to the divergent η_r results among various mixtures. In addition, it is also noticeable that sand with higher sphericity (lower aspect ratio and higher convexity perimeter ratio), provides lower relative plastic viscosity at each PFT. Specifically, the mixture with GB has the lowest η_r and shows negligible increase until PFT decreases to around 100 μm. Therefore, it seems that the influence of geometric features and particle size cannot be explained by their influences on the PFT.

Rather than the average paste thickness considered in most literature, some researchers proposed that the paste film thickness values of the matrix surrounding the particles with various sizes are not identical and instead they may be proportional to the particle sizes [79,80]. The relative paste film thickness (R_PFT) is calculated as the ratio between PFT and the average diameter of sand. The average diameter is determined as $\sqrt{D_{max}D_{min}}$, where D_{max} and D_{min} are the maximum and minimum diameters of each kind of particles.

The variations of relative plastic viscosity with R_PFT are shown in Fig. 14. Similar to the trend shown in Fig. 13, η_r increases with the decrease of R_PFT. It needs to be mentioned that all mixtures show a relatively low η_r when R_PFT is higher than around 0.30, below which η_r presents a drastic increase as the R_PFT decreases. In addition, non-spherical MS particles provide higher η_r compared to spherical GB at each R_PFT. It is acknowledged that the plastic viscosity of mortar mixture is mainly influenced by hydrodynamic force at high R_PFT (low volume fraction) while no collision between particles happens. As the R_PFT decreases, the probability of collision increases, which significantly increases plastic viscosity of mixtures. Specifically, the non-spherical shape of MS increases the hydrodynamic force, consequently increasing the plastic viscosity of mortar at high R_PFT. Besides, non-spherical particles require higher R_PFT to avoid potential interactions than that of spherical particle in that the orbit of a rotating non-spherical particle encloses higher volume of paste. Therefore, a drastic increase of η_r is reached at higher R_PFT for mixtures with MS than mixtures with GB.where T_r is equal to R_PFT, and K is a constant.

The regressions of scatters in Fig. 14 are shown as solid lines, with regression parameters listed in Table 5. It can be seen that excellent regressions are achieved based on Eq. (18). Such higher R^2 values further indicate that R_PFT is the most important parameter governing the relative plastic viscosity of mortar with MS.

It is of great interest that η_r of mixtures with MS presents good convergence with both relative volume fraction and R_PFT from the comparison between Figs. 12 and 14. The η_r results in the red zones in Fig. 14 are employed to compare the dependence of η_r on relative

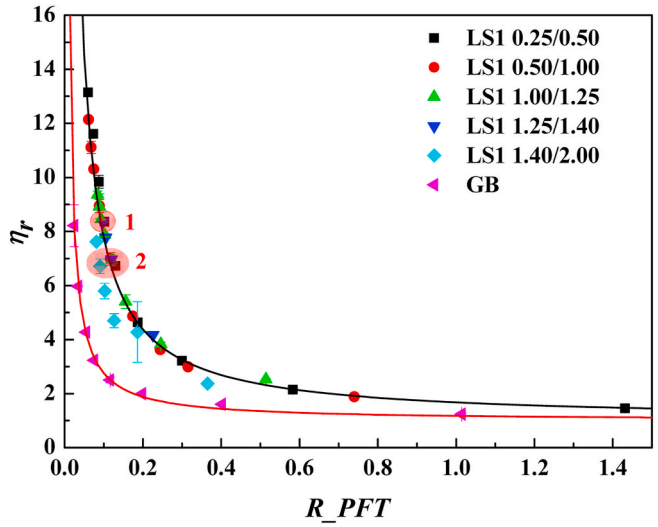

Fig. 14. Relative plastic viscosity of mixtures with various R_PFT. From the mathematical viewpoint, η_r shows a power relationship with R_PFT, expressed as Eq. (18).

$$\eta_r = \frac{K}{T_r} + 1 \tag{18}$$

Table 5
Regression parameters of η_r versus R_PFT.

Sand type	K	R^2
MS	0.641	0.933
GB	0.176	0.998

volume fraction and R_PFT. The variations of the relative volume fraction and R_PFT are normalized by their total ranges in this study, 0.80 and 1.50 respectively. The normalized variations of relative volume fraction and R_PFT are shown in Table 6. Appreciably, for the superimposed points in zone 1, they share the identical η_r of 8.4 while they have the same R_PFT, manifested by the normalized variation of 0. However, their corresponding relative volume fractions vary a lot with the 7.5% normalized variation. Similarly, the data points in zone 2 have a narrow range of η_r, from 6.7 to 7.0. They have a small normalized variation of R_PFT (2.0%) but a higher normalized variation of relative volume fraction (8.8%). Thus, it can be inferred that the η_r shows higher dependence on the R_PFT than on the relative volume fraction of sand. This is reasonable since the R_PFT takes into account the influences of geometric and dimension of particles on both packing properties and surface area while only the influence on packing properties is considered for the relative volume fraction. Therefore, the R_PFT presents priority than the relative volume fraction in terms of dominating the relative plastic viscosity of mortar mixtures. The dependence of η_r on the geometric features and particle size of MS can be attributed to their influences on both the packing fraction and specific surface area of particles.

It needs to be mentioned that the above analysis does not consider influences of geometric features and particle size (distribution) on the hydrodynamic and collision forces. That is why the analysis based on the R_PFT does not encompass both the GB and MS particles. The analysis on the hydrodynamic and collision forces needs to be performed by a numerical simulation study, which will be carried out in a further research study.

In addition, the suspending phase in this study is pure cement paste without chemical admixtures. However, chemical admixtures, especially superplasticizers, have become an indispensable constituent of modern concrete. MS may have adsorption capacity of superplasticizers, depending on the lithology of MS. If MS has no adsorption ability of superplasticizers, the relative plastic viscosity and R_PFT is applicable. Otherwise, modifications need to be performed. Therefore, it is recommended that further research be carried out to understanding the rheology of superplasticized mortar and concrete with MS of various lithologies.

Table 6
η_r of mixtures with respect to their relative volume fractions of sand and R_PFT.

Zone	η_r	Relative volume fraction		R_PFT	
		Variation	Normalized variation (%)	Variation	Normalized variation (%)
1	8.4	0.63–0.69	7.5	0.10	0
2	6.7–7.0	0.58–0.65	8.8	0.09–0.12	2.0

5. Conclusion

In this paper, the geometric features, including overall shape, angularity and roughness, of MS with various sizes were measured by aspect ratio, convexity area ratio, convexity perimeter ratio and circularity. The relative plastic viscosity of mortar mixtures was measured to evaluate the influence of MS from the viewpoints of packing fraction, PFT, and R_PFT. The main conclusions can be drawn as follows.

MS particles have remarkable anisotropy in overall shape with the aspect ratio higher than 2.0, especially for coarser particles. Besides, coarser MS particles have rougher surface while negligible influence is observed in terms of angularity among MS particles. The combined effects of overall shape, angularity and roughness provide coarser MS with lower circularity.

From the viewpoint of packing fraction, shear-induced orientation increases the packing fraction of non-spherical MS particles from the random loose packing fraction. The improvement is increasingly prominent with the decrease of circularity.

Generally, mixtures with MS have higher relative plastic viscosity than mixtures with GB at each volume fraction due to the influence of geometric features of MS on the hydrodynamic force and collision probability. Besides, the higher relative plastic viscosity of mixtures with MS of higher anisotropy (higher aspect ratio, lower convexity, lower circularity) can be attributed to the predomination of the size effect of fine particles over their geometric features.

The favorable convergence of relative plastic viscosity as a function of relative volume fraction, among mixtures with MS demonstrates that geometric features and dimension of MS may influence the rheology via their influences on the packing fraction. While expressed as the function of R_PFT, the relative plastic viscosity of mixtures with MS converges into a single curve. The quantitative analysis shows that the R_PFT is the most significant factor governing the relative plastic viscosity of mortar with MS. The dependence of plastic viscosity of cement mortar on geometric features and particle size of MS can be attributed to their influences on the packing fraction and surface area of particles.

Declaration of competing interest

The authors declare that they have no known competing financial interests or personal relationships that could have appeared to influence the work reported in this paper.

Acknowledgement

The authors gratefully acknowledge the financial supports provided by National Key Research and Development Projects of China (2018YFC0705404), National Natural Science Foundation of China (51878480, 51678442, 51878481 and 51878496), the Fundamental Research Funds for the Central Universities, and the China Scholarship

Council (CSC).

References

[1] D.D. Cortes, H.K. Kim, A.M. Palomino, J.C. Santamarina, Rheological and mechanical properties of mortars prepared with natural and manufactured sands, Cement Concr. Res. 38 (10) (2008) 1142–1147, https://doi.org/10.1016/j.cemconres.2008.03.020.

[2] S.L. Leleu, J.R. Valdes, Experimental study of the influence of mineral composition on sand crushing, Geotechnique 57 (3) (2007) 313–317, https://doi.org/10.1680/geot.2007.57.3.313.

[3] J.P. Gonçalves, L.M. Tavares, R.D. Toledo Filho, E.M.R. Fairbairn, E.R. Cunha, Comparison of natural and manufactured fine aggregates in cement mortars, Cement Concr. Res. 37 (6) (2007) 924–932, https://doi.org/10.1016/j.cemconres.2007.03.009.

[4] S. Safiddine, F. Debieb, E.H. Kadri, B. Menadi, H. Soualhi, Effect of crushed sand and limestone crushed sand dust on the rheology of cement mortar, Appl. Rheol. 27 (1) (2017) 12–20, https://doi.org/10.3933/ApplRheol-27-14490.

[5] H. Donza, O. Cabrera, E.F. Irassar, High-strength concrete with different fine aggregate, Cement Concr. Res. 32 (11) (2002) 1755–1761, https://doi.org/10.1016/S0008-8846(02)00860-8.

[6] W.G. Shen, Y. Liu, Z.W. Wang, L.H. Cao, D.L. Wu, Y.J. Wang, X.L. Ji, Influence of manufactured sand's characteristics on its concrete performance, Construct. Build. Mater. 172 (2018) 574–583, https://doi.org/10.1016/j.conbuildmat.2018.03.139.

[7] B.X. Li, G.J. Ke, M.K. Zhou, Influence of manufactured sand characteristics on strength and abrasion resistance of pavement cement concrete, Construct. Build. Mater. 25 (10) (2011) 3849–3853, https://doi.org/10.1016/j.conbuildmat.2011.04.004.

[8] M. Westerholm, Rheology of the Mortar Phase of Concrete with Crushed Aggregate, Luleå University of Technology, Luleå, 2006.

[9] H. Järvenpää, Quality Characteristics of Fine Aggregates and Controlling Their Effects on Concrete, Helsinki University of Technology, Espoo, 2001.

[10] O.A. Cabrera, L.P. Traversa, N.F. Ortega, Effect of crushed sand on mortar and concrete rheology, Mater. Construt. 61 (303) (2011) 401–416, https://doi.org/10.3989/mc.2011.55609.

[11] M. Westerholm, B. Lagerblad, J. Silfwerbrand, E. Forssberg, Influence of fine aggregate characteristics on the rheological properties of mortars, Cement Concr. Compos. 30 (4) (2008) 274–282, https://doi.org/10.1016/j.cemconcomp.2007.08.008.

[12] M.F. Kaplan, The effects of the properties of coarse aggregates on the workability of concrete, Mag. Concr. Res. 10 (29) (1958) 63–74, https://doi.org/10.1680/macr.1958.10.29.63.

[13] H.A. Barnes, J.F. Hutton, K. Walters, An Introduction to Rheology, Elsevier, Amsterdam, 1989.

[14] R. Cepuritis, S. Jacobsen, B. Pedersen, E. Mortsell, Crushed sand in concrete - effect of particle shape in different fractions and filler properties on rheology, Cement Concr. Compos. 71 (2016) 26–41, https://doi.org/10.1016/j.cemconcomp.2016.04.004.

[15] G.C. Cho, J. Dodds, J.C. Santamarina, Particle shape effects on packing density, stiffness, and strength: natural and crushed sands, J. Geotech. Geoenviron. 132 (5) (2006) 591–602. http://doi.org/10.1061/(asce)1090-0241(2006)132:5(591).

[16] E. Masad, J.W. Button, Unified imaging approach for measuring aggregate angularity and texture, Comput.-Aided Civ. Inf. 15 (4) (2000) 273–280, https://doi.org/10.1111/0885-9507.00191.

[17] H. Hafid, G. Ovarlez, F. Toussaint, P.H. Jezequel, N. Roussel, Effect of particle morphological parameters on sand grains packing properties and rheology of model mortars, Cement Concr. Res. 80 (2016) 44–51, https://doi.org/10.1016/j.cemconres.2015.11.002.

[18] O.A. Cabrera, L.P. Traversa, N.F. Ortega, Flowability in crushed sand mortar, Mater. Construt. 60 (300) (2010) 115–130, https://doi.org/10.3989/mc.2010.50909.

[19] S. Mueller, E.W. Llewellin, H.M. Mader, The effect of particle shape on suspension viscosity and implications for magmatic flows, Geophys. Res. Lett. 38 (2011), https://doi.org/10.1029/2011gl047167.

[20] C.T. Kennedy, The design of concrete mixes, J. Proc. 36 (2) (1940) 373–400, https://doi.org/10.14359/8528.

[21] S.G. Oh, T. Noguchi, F. Tomosawa, Toward Mix Design for Rheology of Self-Compacting Concrete, 1st International RILEM Symposium on Self-Compacting Concrete, RILEM Publications, Stockholm, Sweden, 1999, pp. 361–372.

[22] C.L. Hwang, S.L. Hsieh, Y.Y. Chen, The effect of coating thickness on aggregate on the property of SCC by Fuller's ideal curve and error function, in: G. De Schutter, V. Boel (Eds.), 5th International RILEM Symposium on Self-Compacting Concrete, 2007, pp. 83–88. Ghent.

[23] A.K.H. Kwan, W.W.S. Fung, H.H.C. Wong, Water film thickness, flowability and rheology of cement-sand mortar, Adv. Cement Res. 22 (1) (2010) 3–14, https://doi.org/10.1680/adcr.2008.22.1.3.

[24] A.K.H. Kwan, J.J. Chen, Roles of packing density and water film thickness in rheology and strength of cement paste, J. Adv. Concr. Technol. 10 (10) (2012) 332–344, https://doi.org/10.3151/jact.10.332.

[25] H.H.C. Wong, A.K.H. Kwan, Rheology of cement paste: role of excess water to solid surface area ratio, J. Mater. Civ. Eng. 20 (2) (2008) 189–197. http://doi.org/10.1061/(asce)0899-1561(2008)20:2(189).

[26] A.K.H. Kwan, L.G. Li, Combined effects of water film thickness and paste film thickness on rheology of mortar, Mater. Struct. 45 (9) (2012) 1359–1374, https://doi.org/10.1617/s11527-012-9837-y.

[27] Y. Zhang, Z. Jiang, Y. Zhu, J. Zhang, Q. Ren, T. Huang, Effects of redispersible polymer powders on the structural build-up of 3D printing cement paste with and without hydroxypropyl methylcellulose, Construct. Build. Mater. (2020) 120551, https://doi.org/10.1016/j.conbuildmat.2020.120551.

[28] Y. Chen, J.X. Wei, F.X. Li, J. Hu, Q.J. Yu, Effect of the paste coating layer and mortar coating layer on the properties of fresh self-compacting concrete, J. Sustain. Cem.-Based Mater. 4 (3–4) (2015) 194–204, https://doi.org/10.1080/21650373.2015.1018984.

[29] A.K.H. Kwan, L.G. Li, Combined effects of water film, paste film and mortar film thicknesses on fresh properties of concrete, Construct. Build. Mater. 50 (2014) 598–608, https://doi.org/10.1016/j.conbuildmat.2013.10.014.

[30] D. Jiao, C. Shi, Q. Yuan, X. An, Y. Liu, H. Li, Effect of constituents on rheological properties of fresh concrete-A review, Cement Concr. Compos. 83 (2017) 146–159, https://doi.org/10.1016/j.cemconcomp.2017.07.016.

[31] BS EN 1097-3, Tests for Mechanical and Physical Properties of Aggregates—Part 3: Determination of Loose Bulk Density and Voids, British Standards Institution, London, 1998.

[32] F. de Larrard, T. Sedran, Optimization of ultra-high-performance concrete by the use of a packing model, Cement Concr. Res. 24 (6) (1994) 997–1009, https://doi.org/10.1016/0008-8846(94)90022-1.

[33] ISO 679, Cement-Test Methods-Determination for Strength, International Organization for Standardization, Geneva, 2009.

[34] C.F. Mora, A.K.H. Kwan, Sphericity, shape factor, and convexity measurement of coarse aggregate for concrete using digital image processing, Cement Concr. Res. 30 (3) (2000) 351–358, https://doi.org/10.1016/S0008-8846(99)00259-8.

[35] F.L. Liu, H.Y. Fang, S.J. Chen, L. Zhou, J.H. Yang, Experimental study on manufactured sand shape detection by image method, J. Test. Eval. 47 (5) (2019) 3515–3532, https://doi.org/10.1520/jte20170533.

[36] F. Altuhafi, C. O'Sullivan, I. Cavarretta, Analysis of an image-based method to quantify the size and shape of sand particles, J. Geotech. Geoenviron. 139 (8) (2013) 1290–1307, https://doi.org/10.1061/(ASCE)GT.1943-5606.0000855.

[37] S.T. Erdogan, A.M. Forster, P.E. Stutzman, E.J. Garboczi, Particle-based characterization of Ottawa sand: shape, size, mineralogy, and elastic moduli, Cement Concr. Compos. 83 (2017) 36–44, https://doi.org/10.1016/j.cemconcomp.2017.07.003.

[38] W.B. Zheng, X.L. Hu, D.D. Tannant, Shape characterization of fragmented sand grains via X-ray computed tomography imaging, Int. J. Geom. 20 (3) (2020), 04020003, https://doi.org/10.1061/(asce)gm.1943-5622.0001599.

[39] D. Su, W.M. Yan, 3D characterization of general-shape sand particles using microfocus X-ray computed tomography and spherical harmonic functions, and particle regeneration using multivariate random vector, Powder Technol. 323 (2018) 8–23, https://doi.org/10.1016/j.powtec.2017.09.030.

[40] A.K.H. Kwan, C.F. Mora, H.C. Chan, Particle shape analysis of coarse aggregate using digital image processing, Cement Concr. Res. 29 (9) (1999) 1403–1410, https://doi.org/10.1016/S0008-8846(99)00105-2.

[41] T. Fletcher, C. Chandan, E. Masad, K. Sivakumar, Aggregate imaging system for characterizing the shape of fine and coarse aggregates, Transport. Res. Rec. 1832 (1) (2003) 67–77, https://doi.org/10.3141/1832-09.

[42] T. Al-Rousan, E. Masad, E. Tutumluer, T. Pan, Evaluation of image analysis techniques for quantifying aggregate shape characteristics, Construct. Build. Mater. 21 (5) (2007) 978–990, https://doi.org/10.1016/j.conbuildmat.2006.03.005.

[43] M.A. Taylor, E.J. Garboczi, S.T. Erdogan, D.W. Fowler, Some properties of irregular 3-D particles, Powder Technol. 162 (1) (2006) 1–15, https://doi.org/10.1016/j.powtec.2005.10.013.

[44] P.J. Barrett, The shape of rock particles, a critical review, Sedimentology 27 (3) (1980) 291–303, https://doi.org/10.1111/j.1365-3091.1980.tb01179.x.

[45] L. Wang, W. Sun, E. Tutumluer, C. Druta, Evaluation of aggregate imaging techniques for quantification of morphological characteristics, Transport. Res. Rec. 2335 (1) (2013) 39–49, https://doi.org/10.3141/2335-05.

[46] W.G. Shen, Z.G. Yang, L.H. Cao, L. Cao, Y. Liu, H. Yang, Z.L. Lu, J. Bai, Characterization of manufactured sand: particle shape, surface texture and behavior in concrete, Construct. Build. Mater. 114 (2016) 595–601, https://doi.org/10.1016/j.conbuildmat.2016.03.201.

[47] Q. Ren, G. De Schutter, Z. Jiang, Q. Chen, Multi-level diffusion model for manufactured sand mortar considering particle shape and limestone powder effects, Construct. Build. Mater. 207 (2019) 218–227, https://doi.org/10.1016/j.conbuildmat.2019.02.139.

[48] L. Wang, J.-Y. Park, Y. Fu, Representation of real particles for DEM simulation using X-ray tomography, Construct. Build. Mater. 21 (2) (2007) 338–346, https://doi.org/10.1016/j.conbuildmat.2005.08.013.

[49] L. Liu, D. Shen, H. Chen, W. Xu, Aggregate shape effect on the diffusivity of mortar: a 3D numerical investigation by random packing models of ellipsoidal particles and of convex polyhedral particles, Comput. Struct. 144 (2014) 40–51, https://doi.org/10.1016/j.compstruc.2014.07.022.

[50] C.-Y. Kuo, R.B. Freeman, Imaging indices for quantification of shape, angularity, and surface texture of aggregates, Transport. Res. Rec. 1721 (1) (2000) 57–65, https://doi.org/10.3141/1721-07.

[51] D. van Lent, A. Molenaar, M. van de Ven, Influence treatment in laboratory of stone surface on the surface roughness, J. Test. Eval. 37 (5) (2009) 417–423, https://doi.org/10.1520/JTE000017.

[52] L. Wang, J. Frost David, Quantification of the specific aggregate surface area using X-ray tomography, in: E. Tutumluer, Y.M. Najjar, E. Masad (Eds.), 15th Engineering Mechanics Division Conference, ASCE, New York, United States, 2002, pp. 3–17, https://doi.org/10.1061/40709(257)1.

[53] Q. Ren, L. Ding, X. Dai, Z. Jiang, G. Ye, G. De Schutter, Determination of specific surface area of irregular aggregate by random sectioning and its comparison with

conventional methods, Construct. Build. Mater. 273 (2021), 122019, https://doi.org/10.1016/j.conbuildmat.2020.122019.
[54] Z. Toutou, N. Roussel, Multi scale experimental study of concrete rheology: from water scale to gravel scale, Mater. Struct. 39 (2) (2006) 189–199, https://doi.org/10.1617/s11527-005-9047-y.
[55] P.F.G. Banfill, Rheological methods for assessing the flow properties of mortar and related materials, Construct. Build. Mater. 8 (1) (1994) 43–50, https://doi.org/10.1016/0950-0618(94)90007-8.
[56] A. Einstein, Eine neue bestimmung der moleküldimensionen, Ann. Phys.-Berl. 324 (2) (1906) 289–306.
[57] J. Yammine, M. Chaouche, M. Guerinet, M. Moranville, N. Roussel, From ordinary rhelogy concrete to self compacting concrete: a transition between frictional and hydrodynamic interactions, Cement Concr. Res. 38 (7) (2008) 890–896, https://doi.org/10.1016/j.cemconres.2008.03.011.
[58] I.M. Krieger, T.J. Dougherty, A mechanism for non-Newtonian flow in suspensions of rigid spheres, Trans. Soc. Rheol. 3 (1) (1959) 137–152, https://doi.org/10.1122/1.548848.
[59] M. Mooney, The viscosity of a concentrated suspension of spherical particles, J. Colloid Sci. 6 (2) (1951) 162–170, https://doi.org/10.1016/0095-8522(51)90036-0.
[60] S.H. Maron, P.E. Pierce, Application of Ree-Eyring generalized flow theory to suspensions of spherical particles, J. Colloid Sci. 11 (1) (1956) 80–95, https://doi.org/10.1016/0095-8522(56)90023-X.
[61] D. Quemada, Rheology of concentrated disperse systems and minimum energy dissipation principle, Rheol. Acta 16 (1) (1977) 82–94, https://doi.org/10.1007/bf01516932.
[62] J.V. Robinson, The viscosity of suspensions of spheres, J. Phys. Chem. 53 (7) (1949) 1042–1056, https://doi.org/10.1021/j150472a007.
[63] H. Eilers, Die viskosität von emulsionen hochviskoser stoffe als funktion der konzentration, Kolloid Z. 97 (3) (1941) 313–321, https://doi.org/10.1007/BF01503023.
[64] J.J. Stickel, R.L. Powell, Fluid mechanics and rheology of dense suspensions, Annu. Rev. Fluid Mech. 37 (2005) 129–149, https://doi.org/10.1146/annurev.fluid.36.050802.122132.
[65] J.M. Brader, Nonlinear rheology of colloidal dispersions, J. Phys.-Condens. Mat. 22 (36) (2010) 363101, https://doi.org/10.1088/0953-8984/22/36/363101.
[66] X. Chateau, G. Ovarlez, K.L. Trung, Homogenization approach to the behavior of suspensions of noncolloidal particles in yield stress fluids, J. Rheol. 52 (2) (2008) 489–506, https://doi.org/10.1122/1.2838254.
[67] F.O. Marques, N. Mandal, R. Taborda, J.V. Antunes, S. Bose, The behaviour of deformable and non-deformable inclusions in viscous flow, Earth Sci. Rev. 134 (2014) 16–69, https://doi.org/10.1016/j.earscirev.2014.03.007.
[68] S. Mueller, E.W. Llewellin, H.M. Mader, The rheology of suspensions of solid particles, P. Roy. Soc. A-Math. Phys. 466 (2116) (2010) 1201–1228, https://doi.org/10.1098/rspa.2009.0445.
[69] P.M. Chaikin, A. Donev, W.N. Man, F.H. Stillinger, S. Torquato, Some observations on the random packing of hard ellipsoids, Ind. Eng. Chem. Res. 45 (21) (2006) 6960–6965, https://doi.org/10.1021/ie060032g.
[70] S. Wegner, R. Stannarius, A. Boese, G. Rose, B. Szabo, E. Somfai, T. Borzsonyi, Effects of grain shape on packing and dilatancy of sheared granular materials, Soft Matter 10 (28) (2014) 5157–5167, https://doi.org/10.1039/c4sm00838c.
[71] D.Z. Gunes, R. Scirocco, J. Mewis, J. Vermant, Flow-induced orientation of non-spherical particles: effect of aspect ratio and medium rheology, J. Non-Newton. Fluid 155 (1–2) (2008) 39–50, https://doi.org/10.1016/j.jnnfm.2008.05.003.
[72] T.C. Powers, The Properties of Fresh Concrete, John Wiley & Sons, New York, 1968.
[73] Y. Ghasemi, M. Emborg, A. Cwirzen, Exploring the relation between the flow of mortar and specific surface area of its constituents, Construct. Build. Mater. 211 (2019) 492–501, https://doi.org/10.1016/j.conbuildmat.2019.03.260.
[74] A. Ganaw, A. Ashour, Rheological properties of mortars prepared with different sands, ACI Mater. J. 111 (5) (2014) 561–568.
[75] S. Nishibayashi, A. Yoshino, S. Inoue, T. Kuroda, Effect of properties of mix constituents on rheological constants of self-compacting concrete, in: P.J.M. Bartos, D.J. Cleland, D.L. Marrs (Eds.), Production Methods and Workability of Concrete, CRC Press, Scotland, 1996, pp. 267–274.
[76] V.K. Bui, Y. Akkaya, S.P. Shah, Rheological model for self-consolidating concrete, ACI Mater. J. 99 (6) (2002) 549–559.
[77] C.F. Ferraris, J.M. Gaidis, Connection between the rheology of concrete and rheology of cement paste, ACI Mater. J. 89 (4) (1992) 388–393.
[78] J.H. Lee, J.H. Kim, J.Y. Yoon, Prediction of the yield stress of concrete considering the thickness of excess paste layer, Construct. Build. Mater. 173 (2018) 411–418, https://doi.org/10.1016/j.conbuildmat.2018.03.124.
[79] W.Q. Zuo, J.P. Liu, Q. Tian, W. Xu, W. She, P. Feng, C.W. Miao, Optimum design of low-binder self-compacting concrete based on particle packing theories, Construct. Build. Mater. 163 (2018) 938–948, https://doi.org/10.1016/j.conbuildmat.2017.12.167.
[80] K.K. Daddy, P. Diederich, A. Yahia, M. Chekired, Influence of Shape, Size, and Solid Concentration of Particles on Rheological Properties of Self-Consolidating Mortar, 2016, p. 439. Washington DC, USA 15-18 May 2016 Edited by Kamal H. Khayat.